Exploration of a Na3V2(PO4)3/C –Pb full cell Na-ion prototype

Bidhan Pandit, Moulay-Tahar Sougrati, Bernard Fraisse, Laure Monconduit

Exploration of a $Na_3V_2(PO_4)_3$/C –Pb full cell Na-ion prototype

Bidhan Pandit[a], Moulay Tahar Sougrati[a,b], Bernard Fraisse[a], Laure Monconduit[a, b,*]

[a]*ICGM, Univ. Montpellier, CNRS, ENSCM, Montpellier, France*

[b]*Réseau sur le Stockage Electrochimique de l'Energie (RS2E), FR CNRS 3459, Hub de l'Energie, Amiens, France*

***Corresponding Author**: laure.monconduit@umontpellier.fr

Abstract

Recent research focusses typically on sodium-ion half cells, and the progress of high performance and cost-effective full cells remain a critical obstacle to commercialize sodium-ion batteries. Here, we rationally designed a full sodium-ion battery based on $Na_3V_2(PO_4)_3$ (NVP-C) cathode and Pb anode materials. Carbon coated NVP-C is prepared via easy and one-step solid-state method. With 8 wt% carbon content, the obtained NVP-C core-shell structure provides an excellent reversible capacity of 104 mAh/g at C/10 rate, approaching its theoretical capacity. The NVP-C electrode even at a high 10C rate delivers a primary reversible capacity of 87 mAh/g with 99.9% capacity retention almost after 3500 cycles. As an anode, Pb delivers an initial reversible capacity of 477 mAh/g at a fixed current density of 13 mA/g with a good cyclability and capacity retention of 98.5% over 50 cycles. From the as prepared materials a full cell was achieved, which exhibited a preliminary reversible capacity of 233 mAh/g at C/10. In addition, the good rate capability including discharge energy density in the range of 170-180 Wh/kg brands the full cell a potential candidate in practical sodium-ion battery application. The excellent electrochemical behavior with simple, low-cost properties of fabricated full cell mark it as attractive option for high-energy and energy storage applications.

Keywords:

Sodium-ion battery, cathode material, polyanionic phosphates, $Na_3V_2(PO_4)_3$-C, full cell, lead anode

1. Introduction

Owing to their excellent electrochemical performance rechargeable lithium-ion batteries (LIBs) become, over the past several decades, an indispensable energy storage device in the world [1-3]. Though, the advancement of LIBs yet experiences strong issues such as limited cobalt and lithium sustainability and safety issues. The limited abundance and especially the uneven distribution of lithium, added to the emerging huge demand for electrical energy storage, could increase the cost and limit the sustainability of lithium. Sodium-ion batteries (SIBs), however still in early stages of its development, are comparatively appropriate for grid storage applications with large-scale integration as associated with low cost precursors and abundance properties of sodium (4^{th} most abundant element in the Earth) [4, 5] and the possibility to substitute the copper into aluminium in current collectors. It is important to advance new and novel electrode materials for high-performance SIBs.

In the past few years, a wide array of cathode materials such as transition metal oxides [6-11], phosphates [12-14], and ferrocyanides [15, 16] has been investigated for sodium-ion batteries (SIBs) with moderate operating voltage (~3.0 V) [17]. The polyanionic phosphate materials have attracted a great attention as cathode materials for SIBs due to stable reversibility and high redox voltage. In this regard, Na^+ superionic conductor (NASICON) materials have been explored as potential cathodes for SIBs. Normally, NASICON materials are well insertion hosts with the structure of $Na_xM_2(XO_4)_3$, where M = Ti, V, or Fe; and X = S, P, Mo, W, or As. Rhombohedral $Na_3V_2(PO_4)_3$ (NVP) provides excellent ionic mobility and great theoretical capacity (117.6 mAh/g) with high redox voltage. Moreover, NVP accommodates Na ions in the interstitial sites with three-dimensional (3D) framework of PO_4 tetrahedra and VO_6 octahedra sharing the oxygen. Though, the less conductivity which is because of the dissociation of PO_4 tetrahedra from VO_6 octahedra in rhombohedral structure,

restricts its rate capability and cycling ability. Many strategies have been adapted to get over it, such as, decreasing particle size [18, 19] metal ionic doping [20-22], morphology designing [23, 24], and most importantly carbon coating [25-29]. The NVP-C core–shell nanostructure with thin carbon layer coating on NVP nanoparticles is favorable due to enhanced electron conduction with instantaneously smaller diffusion length for the associated Na^+ ions. Though, the synthesis of NVP-C core-shell structure is difficult, because the preparation of large poly-phosphate framework normally includes calcination course at high temperature, in which the core has a tendency to grow and cumulate into big grain sized particles [29-31].

On the anode side for SIB, although graphite associates with poor Na-ion insertion, hard carbon (HC) can assist an excellent capacity of 300 mAh/g because of the complex mechanism including pseudocapacitive activities, but is a costly material. Many candidates have been proposed during the last decade including intercalation, conversion and alloying materials. Among the alloying materials, lead (Pb) has the advantage of being the most recycled metal since it recycling reaches even more than 99% (one of the uppermost recycling rates in the earth where no other metal is managed with a such higher sustainability). Up to now, lead-acid batteries are the most-reported, and widely used system compared to other batteries. As newly battery technologies (ion batteries) are introduced, lead-acid batteries are now side-lined by them. Though, Pb was generally not supported as feasible anode material for alkali-ion battery applications due to its toxicity, and only few report can be found regarding Pb-based anode materials for Li [32], Na [33] and K-ion [34]. Moreover, Pb based composite such as $Pb(NO_3)_2$/CNT shows potential sodium storage as reported by Lin et al. [35]. Pb as alloy anode has however shown higher gravimetric and volumetric capacities than traditional carbonaceous anodes [36-38].

In this work, we prepared $Na_3V_2(PO_4)_3$ using a facile one-step solid-state method and prepared an efficient Pb based electrode to finally build a NVP/Pb SIB. The mechanism of sodiation/desodiation was studied in both materials. The performance of the NVP/Pb battery was evaluated at different rates. The performance of this new SIB is encouraging, and could become an elegant way to recycle the classical lead-acid batteries into anode material for potential Na-ion batteries.

2. Experimental details

2.1 Synthesis

10 mmol of V_2O_5 (99.9%, Alpha), 30 mmol of $NaH_2PO_4 \cdot 2H_2O$ (99.9%, Alpha), and 2.5g of sugar (2.5 g) were mixed at 1000 rpm in a stainless steel vessel for 2 hours using SPEX ball mill. After the ball milling process, the obtained mixture was pressed into pellets and calcined at 800 ° C for 24 h under argon flow.

2.2 Material characterization

Powder X-ray diffraction (XRD) was carried out via Bruker D8 Advance diffractometer with monochromatic CuK_α radiation (λ = 1.5406 Å). The X-ray Rietveld refinement was completed using FullProf program with the help of the pseudo-Voigt function. laser excitation of 532 nm equipped with LabRAM HR was engaged for Raman studies. The X-ray photoelectron spectroscopy (XPS) analysis was examined with the help of ESCALAB 250 (ThermoElectron) spectrometer with Al Kα excitation source (1486.6 eV). The morphology and composition of the nanostructures were examined via field emission scanning electron microscope (FESEM, Hitachi S-4800) and high-resolution transmission electron microscope (HRTEM, TECNAI G2 20 Twin, FEI).

2.3 Electrochemical characterization

The electrochemical properties of (NVP-C) electrode as cathode was investigated by standard coin cells fabricated in glove box (argon-filled). The associated electrode was formulated using Polyvinylidene fluoride (PVdF) (Solef 5130, Solvay) binder and a uniform mixture (1:1) of vapor grown carbon fibers (VGCF-H) and carbon black as conductive additive, altogether in 1-Methyl-2-pyrrolidinone (NMP) (99.5% Sigma Aldrich) solvent. A slurry associating with active material (70%wt), conductive additive (18%wt) and binder (12%wt) was equally mixed using planetary ball-milling (1 h), tape-casted on aluminium foil substrate, initially dried at normal atmosphere and eventually at 80 °C under vacuum for 12h [39]. The active electrode mass in the prepared electrode is varied between 2 and 10 mg/cm^2.

The electrochemical tests were executed by using metallic sodium (sigma Aldrich) as counter-electrode and 1 M $NaPF_6$ in diglyme as electrolyte, and whatman glass-fiber as separator. The choice of diglyme is imposed by the anode material which offers the best performance with this special electrolyte. The electrochemical tests were executed at 25 °C by using MPG system. For *in situ* XRD investigation, the electrode was fabricated on aluminium collector using the *in situ* cell as reported previously [40]. The cell was cycled at low C/10 rate (one Na^+ extraction/insertion in 10 h), and the interval among two successive XRD patterns associates with 0.1 extracted/inserted Na^+.

Full cells were fabricated with NVP-C as cathode material and Pb as anode material. The micrometric Pb powder (99.95%, Sigma Aldrich) was used without any further treatment. Like cathode, same material and procedure were considered to prepare anode electrode. However, the electrode formulation ratio was 98:1:1 for active material, conductive additive and binder, respectively. The $m_{cathode}/m_{anode}$ mass ratio for full coin cell was eventually chosen at 4.8:1 (capacity balance as specified by half-cell performance), considering for this purpose the mass of the positive electrode should be higher than negative electrode to provide sufficient sodium supply.

3. Results and discussion

3.1 NVP synthesis and characterization

The XRD refined pattern (by using Fullprof software) [41] of the as-synthesized NVP-C is depicted in **Fig. 1a**. All the intense and well-defined peaks of XRD indicates to rhombohedral $Na_3V_2(PO_4)_3$ structure (space group: R -3 c) with refined lattice parameters of a=8.7323(2) Å, b=8.7323(2) Å, c=21.8212(7) Å, α=90.00°, β=90.00°, and γ=120.00° in agreement with reported results (COD#96-222-5133) [42]. The Rp and Rwp values for the refinement are 19.7 and 22.8, respectively. The crystal structure of $Na_3V_2(PO_4)_3$ was originally reported by Delmas et al [43].

Tiny diffraction peaks related to unknown impurity by-product phase are observed around 24 and 27°, likely originated from high temperature preparation process.

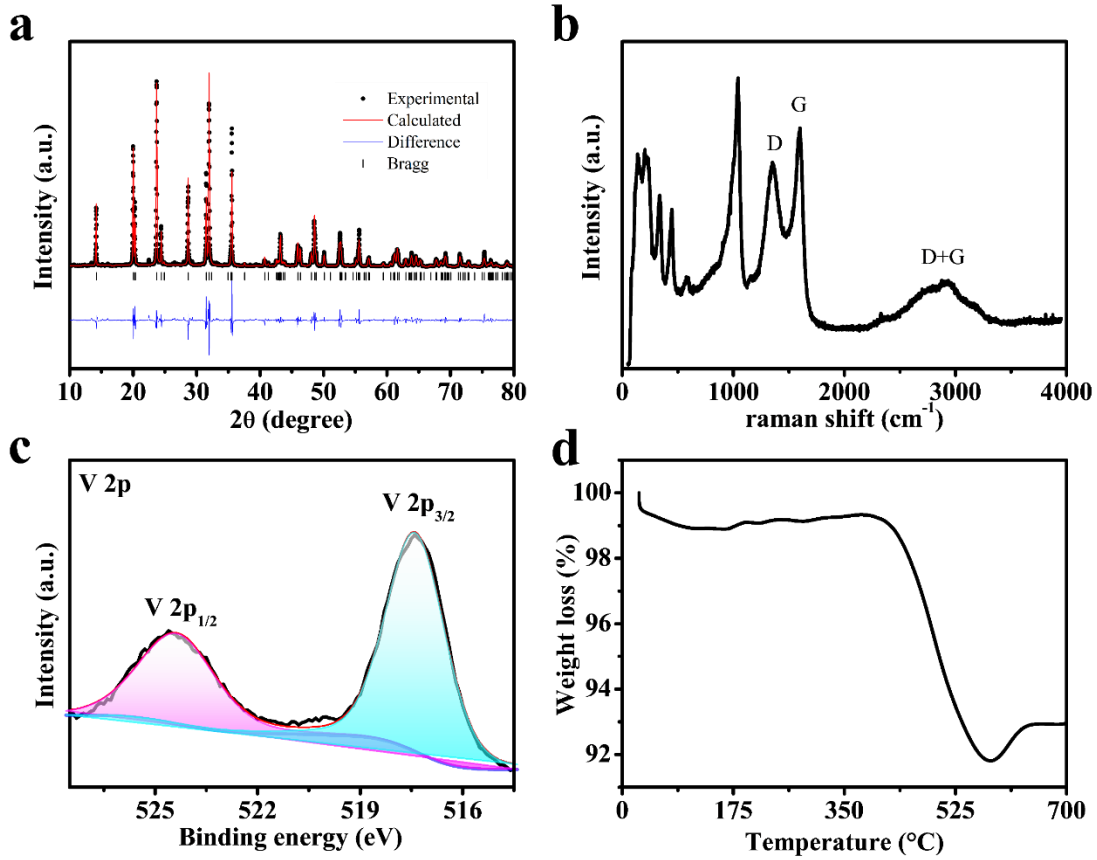

Figure 1 (a) X-ray diffraction powder pattern (CuK_α source) Rietveld refinement, (b) Raman scattering spectrum, (c) High-resolution XPS spectrum, and (d) TG analysis of NVP-C powder.

Raman spectrum was examined to analyse the nature of the associated carbon present in NVP-C material (**Fig. 1b**). The sharp peaks at 138, 228, and 333 cm^{-1} are ascribed to the crystalline lattice vibrations [44]. Two distinctive bands located at 1350 and 1605 cm^{-1} correspond to disorder phonon mode (D-band) and E2g vibrations (G-band) of graphite, respectively [45]. Additionally, the bands present at 1040 and 446 cm^{-1}, associate to the stretching vibrations mode of the PO_4 [46, 47]. The peak around 576 cm^{-1} is due to the intramolecular stretching modes of the PO_4^{3-} anion [48]. The broad (D+G) bond refers to the mixed phase combining both the amorphous and graphitic carbon is observed around 2500-3500 cm^{-1} [49]. The peak intensity ratio (I_D/I_G) of D and G bands of 0.86 indicates the moderately disordered carbon nature.

XPS studies were examined to characterize the states of chemical bonds related to NVP-C. The core-level XPS spectrum (**Fig. 1c**) of V 2p forms a doublet for V 2p1/2 and V 2p3/2 at the binding energies of 524.4 and 517.3 eV, agreeing to V^{3+} oxidation state [50-52]. The poor peak detected at 519.3 eV is allocated to the satellite peak of O 1s [53].

The thermogravimetric (TG) data were collected up to 700 °C in air to calculate the associated carbon content. As per TG curve (**Fig. 1d**) a first loss of ~1% is observed before 100°C which might be attributed to traces of water adsorbed on NVP particles. The smaller weight gain between 150 and 350 ℃ observed for carbon-coated $Na_3V_2(PO_4)_3$ should be attributed to the slight oxidation of V^{3+} [54]. Similar kind of trend is reported in the literature for NVPC material [42, 55]. The drastic loss of 7 wt.% between 400 and 550°C can be attributed to carbon oxidation. After 600 °C, there is a gain of weight as the core particles participate in oxidation after losing its shell structure.

3.2 Morphological analysis

The morphology of prepared material was examined by SEM, as depicted in **Fig. 2a, b**. SEM images display that $Na_3V_2(PO_4)_3$-C has a core-shell structure with the particle size in the range of 0.2–2 μm. To inspect the elemental composition of NVP-C, energy dispersive X-ray spectroscopy (EDS) spectrum was executed (**Fig. S1**) revealing that the content for NVP-C with element approximate ratio of Na:V:P:O=3:2:3:12, in good agreement with the formation of $Na_3V_2(PO_4)_3$ (**Table S1**).

TEM and HRTEM confirms that the hierarchical architecture of as-prepared material is built including the carbon coating with the nanoshell thickness of around 20 nm, as shown in (**Fig. 2c, d**). It is also observed that the NVP particles has a clear boundary with residual carbon shell developed from sugar pyrolysis process (**Fig. 2d, e**). TEM elemental mapping of NVP-C were alongside investigated (**Fig. 2f-j**), demonstrating the homogeneity of C, Na, V, P, and O elements in each particle and the homogeneous carbon shell.

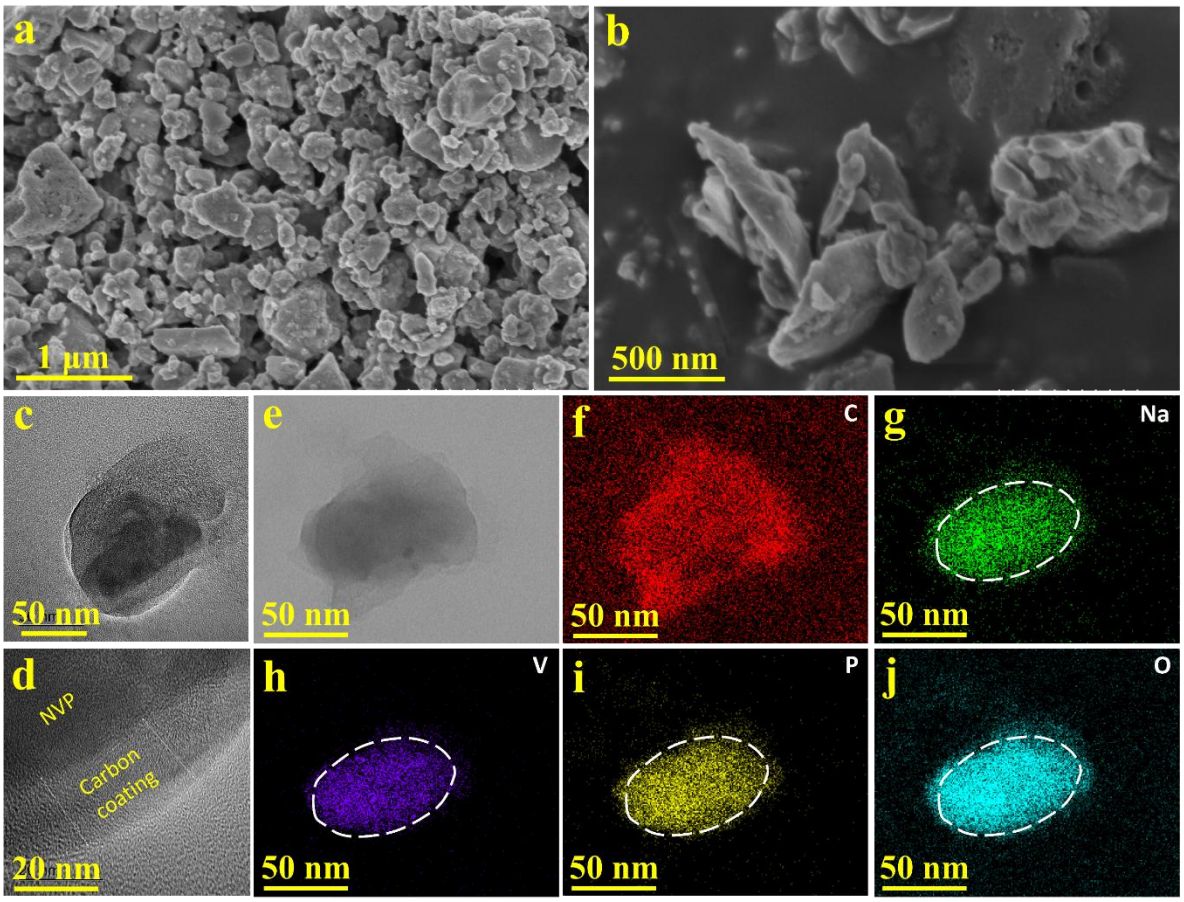

Figure 2 (a, b) FESEM images, (c, d) HRTEM images and (e-j) EDS elemental mapping of NVP-C powder.

3.3 Electrochemical performance of NVP-C cathode

The electrochemical behaviour of the $Na_3V_2^{3+}(PO_4)_3$-C was studied first in half cells vs. Na. **Fig. 3a, b** displays the charge-discharge (CD) data of NVP-C in the voltage window of 3–3.8 V vs. Na^+/Na at C/10 rate (current density of 5.12 mA/g). At this rate, the charge process occurs as a flat plateau around 3.39 V, and corresponds to the extraction of 2 Na^+ (**Fig. 3a**) while the discharge's plateau is at 3.37 V and corresponds to the re-insertion of 2 Na^+, in good agreement with a reversible biphasic reaction [56]. At this rate, the polarization is very low (around 20 mV). The extraction of 2 Na^+ suggests that only the V^{3+}/V^{4+} redox couple can be activated in this potential window. The rather flat plateaus confirm the

occurrence of reversible phase transformation among $Na_3V_2(PO_4)_3$ and $NaV_2(PO_4)_3$ according to these equations:

$$Na_3V_2(PO_4)_3 \underset{\text{Discharge } (+2Na)}{\overset{\text{Charge } (-2Na)}{\leftrightarrow}} NaV_2(PO_4)_3 \qquad (1)$$

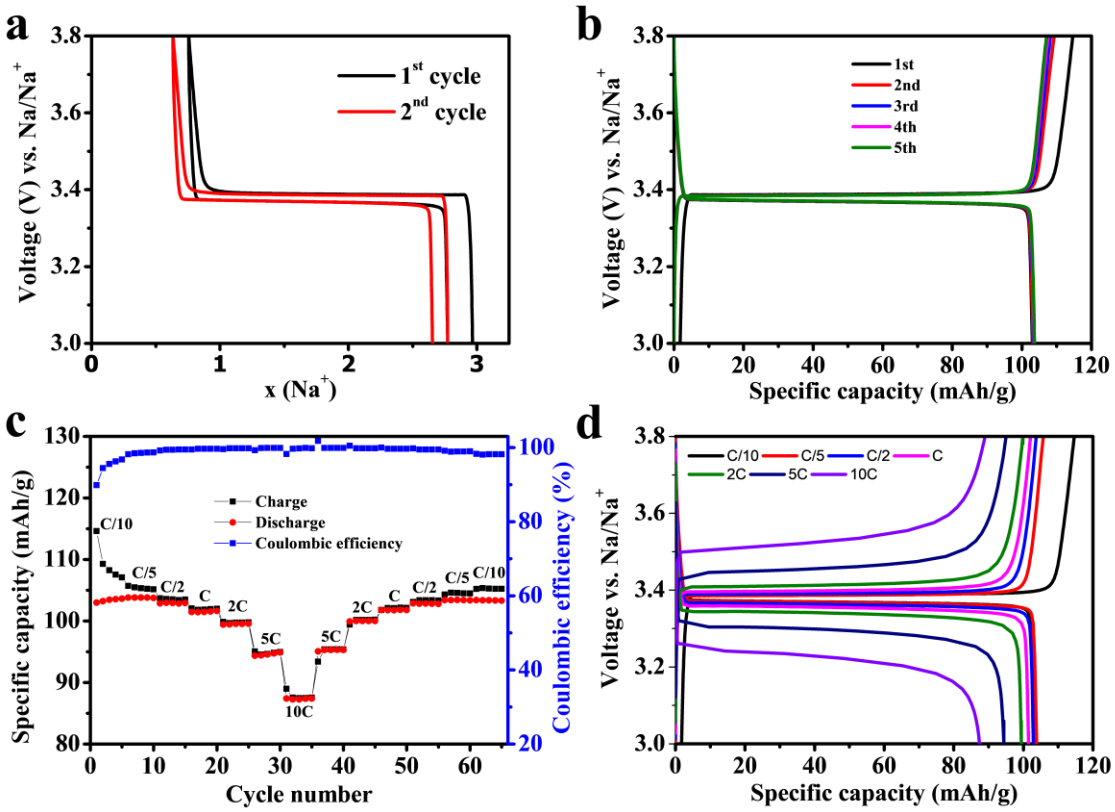

Figure 3 (a) Voltage curves of NVP-C electrode per Na^+ ion at C/10 current rate. (b) Galvanostatic charge-discharge profiles of first five cycles at C/10 current rate. (c) Rate performance at different current rates starting from C/10 and 10C (1 C = 51.2 mA/g). (d) Galvanostatic charge-discharge plots at different current rates.

Fig. 3c compares the specific capacities of NVP-C electrode ranging from C/10 (5.12 mA/g) up to 10C (512 mA/g). The electrode exhibits very high-rate capability with the associated discharge capacities of 104, 103, 102, 101, 99, 94, and 87 mAh/g at the rates of C/10, C/5, C/2, 1C, 2C, 5C, and 10C, respectively. Even at high 10C rate, the NVP-C

electrode is efficient to provide ~85% of its reversible capacity as compared to the capacity obtained at C/10 rate, demonstrating an excellent rate capability of the electrode. When the rate is returned to C/10, the associated electrode sustains almost 100% of the initial capacity highlighting the robustness of NVP framework and its excellent ionic and electronic transport properties. **Fig. 3c and 3d** display the rate capability and the charge−discharge plots of electrode at different C-rates: one notes a slight increase of the voltage polarization appears at high rate **Fig. 3d**, but concomitantly the coulombic efficiency is increased **Fig. 3c**.

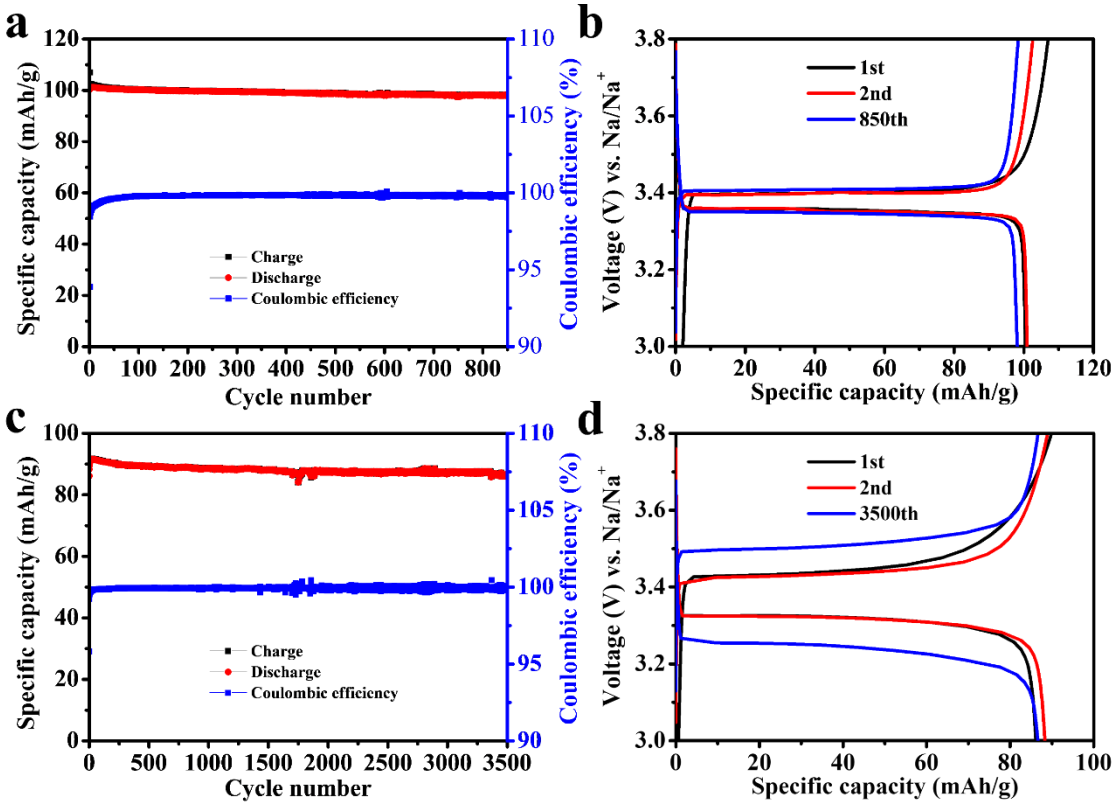

Figure 4 (a) Stability studies and associated coulombic efficiency of NVP-C electrode studied at 1C for 850 cycles. (b) Corresponding galvanostatic charge-discharge profiles. (c) Long-term stability performance and coulombic efficiency at 5C for 3500 cycles. (d) Corresponding galvanostatic charge-discharge profiles.

The long-term cyclic stability of NVP-C electrode was also examined at 1 and 5C rates. In **Fig. 4a**, the early discharge capacity at 1C is 100 mAh/g, and 98% (considering the

highest discharge capacity, generally about 5th cycle) of the associated capacity is maintained even after 850 cycles. Furthermore, the related coulombic efficiency quickly reaches to 99.8% after few cycles and maintained an excellent result throughout the cycling studies. The voltage profiles of NVP-C at various cycles under 1C rate shows a still limited polarization at this rate (**Fig. 4b**). The exceptional cycle durability of the NVP-C cathode is also studied at higher current density of 5C (3500 cycles), as shown in **Fig. 4c**. The first discharge capacity is 86.2 mAh/g at 5C, which slightly increases up to 90 mAh/g during first couple of cycles. After 3500th cycles, the specific capacity is stabilized to 86.1 mAh/g that agrees to 99.9 % of the starting reversible capacity. After 3500 cycles at 5C, although only a very low loss of capacity is measured, an increase of the polarization is observed (**Fig. 4d)** likely due to a decrease of conductivity influenced by the change of Na dynamics and charge-transfer impedance [57]. This remarkable cyclability (3500 cycles) at high current rate signifies the NVP-C cathode as a potential contender for SIB application as compared with previously reported literature (**Fig. 5a, b**).

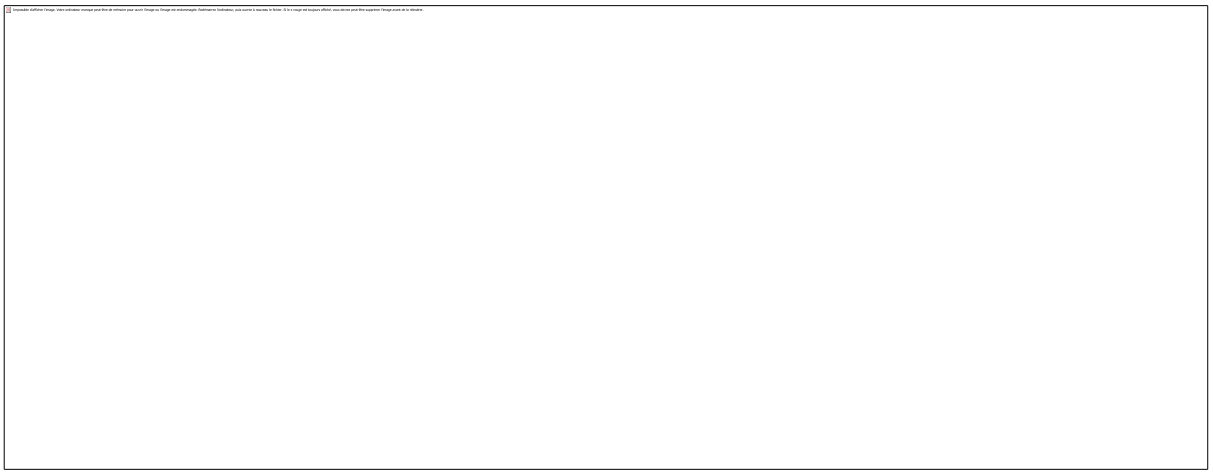

Figure 5 (a, b) Capacity and stability results of our NVP-C half-cell compared with reported literatures.

Here we selected some recently reported high-performance Na ion batteries fabricated with NVP and related composites [58-68]. Some literature shows slightly higher capacities

compared to our electrode (**Table 1**), however none of the previous works showed stable capacities for 3500 cycles.

Table 1: Typical electrochemical performance of NVP-C from previously reported literature.

Material	**Preparation method**	**Carbon source**	**Particle size and morphology**	**Electrode formulation**	**Electrolyte**	**Reversible capacity (mAh/g)**	**Rate (C)**	**$C_{final}/C_{initial}$) (%)**	**Maximum Cycles**	**Ref.**
NVP/C	Sol–gel method	Ascorbic acid	100 to 200 nm particles	80% active + 10% carbon black + 10% PVDF in NMP	1M $NaClO_4$ in PC	98	1	74	450	[58]
NVP/AC	Sol–gel method	Acetylene carbon	nanograins with diameter of ~5 nm	70 % active + 20% carbon black + 10 %PVDF in NMP	1 M $NaClO_4$ in EC+ DMC (1:2)	105	1	96	200	[59]
NVP/C	Two-step solid-state reaction	Glucose	micron-sized particles	80% active + 10% carbon black + 10% PVDF in NMP	1 M NaFSI in EC+PC (1:1)	104	1	89	100	[60]
NVP/C	Sol–gel method	Glycolic acid	nano-sized morphology	80% active + 10% carbon black + 10% PVDF in NMP	1 M $NaClO_4$ in EC+PC (1:1)	~105	1	97	100	[61]
NVP/C	Sol–gel method	Critic acid	particle size about 3–11 µm	80% active + 10% carbon black + 10% PVDF in NMP	1M $NaClO_4$ in EC+DEC (1:1) + 5% FEC	~100	1	98	100	[62]
NVP/C	Carbon-thermal reduction	Glucose	1.0 µm, with irregular morphology	75% active + 15% acetylene black + 10% PVDF in NMP	1 M $NaClO_4$ in PC	95	1	95	50	[63]
NVP/C	Sol–gel method	Acetylene	-	70 % active + 20% acetylene black + 10 %PVDF in NMP	1M $NaClO_4$ in EC+DMC (1:1) + 5% FEC	107	1	86	300	[64]
NVP/C/Ag	Modified Pechini method	Oxalic acid	Particles 200 nm to 5 µm	70% active + 20% carbon black + 10% PVDF in NMP	1 M $NaPF_6$ EC+PC (1:1)	113	1	98	100	[65]

NVP@PEDOT	*In situ* oxidation polymerization	PEDOT	particle is ~500 nm	70 % active + 20% acetylene black + 10 %PVDF in NMP	1M $NaClO_4$ in EC+DEC (1:1)	100	1	93	100	[66]
NVP@C nanofibers	Electrospinning method	Citric acid, PVP	50–200 nm in diameter	75% active + 10% acetylene black + 15% PVDF in NMP	1 M $NaPF_6$ EC+DEC	110	1	93	300	[67]
NVP/C	surfactant-assisted	oleic acid	submicron	80% active + 10% carbon black + 10% PVDF in NMP	1 M $NaPF_6$ EC+DEC (10% FEC)	~100	1	~100	100	[68]
NVP-C	Solid-state	Sugar	100 nm up to a few µm	70% active + 9% C65+ 9% VGCF + 12% PVDF in NMP	1 M $NaPF_6$ in Diglyme	101	1	99.9	3500	Our work

3.4 Reaction mechanism

To establish the reaction mechanism of NVP-C cathode, *operando* XRD analysis was conducted with a special *in situ* cell with cobalt (Co K_α) source in the 2θ range (22°−44°) within the potential window of 3.0−3.8 V at rate of C/10 and the results are depicted in **Fig. 6a**.

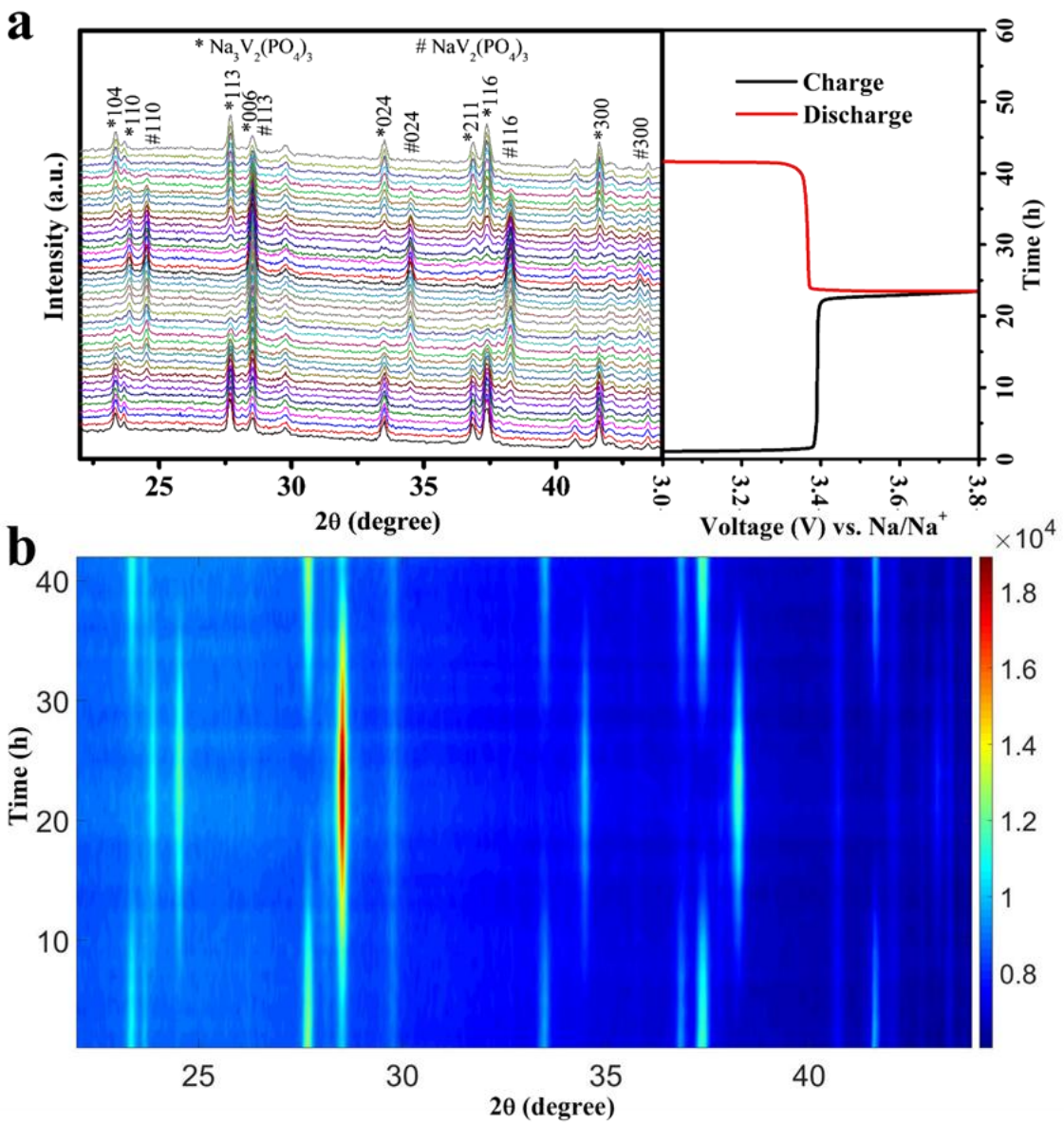

Figure 6 (a) Operando XRD patterns of NVP-C battery during the first cycle at C/10 current rate with cobalt (Co K_α) source, aluminium collector and with beryllium cell window. (b) Contour plot of the operando XRD results.

The associated CD profile of the NVP-C electrode is presented on the right of **Fig. 6a** to observe the change in states with XRD. The associated contour plots of *operando* XRD patterns are also presented in **Fig. 6b**, red and blue colors signify the maximum and minimum intensities of XRD peaks, sequentially. The intensity of NVP peaks (*) are slowly decreases in the charge step starting from OCV to 3.8 V, while new peaks nearby are growing indicating the formation of the well crystalized $NaV_2(PO_4)_3$ (#) [69] (**Fig. S2**) as a typical biphasic reaction in agreement with previous literatures [64, 70, 71]. The pristine NASICON

structure is maintained and only one of the two Na Wyckoff sites (6b and 18e) is occupied (6b). Only two thirds of Na atoms can be electrochemically extracted from NVP structure through the V^{3+}/V^{4+} oxidation process [72, 73], the V^{4+}/V^{5+} redox couple was reported in the NVP around 4 V vs. Na^{+}/Na only in partially Cr [74], Al [75], or Fe [76] substituted NVP.

During initial discharging stage, the intensities of newly developed $NaV_2(PO_4)_3$ phase peaks reduce with the appearance of $Na_3V_2(PO_4)_3$ phase peaks. At the end of full discharge down to 3 V, each and every XRD appeared peaks are recognized to $Na_3V_2(PO_4)_3$, confirming the complete reversibility of the mechanism **(Fig. S2)**.

3.5 Electrochemical performance of Pb//NVP-C full cell

Recently our group has showed that Pb anode for sodium-ion half-cell exhibits i) an excellent reversible capacity of 464 mAh/g with the retention of 98.5 % of its initial capacity after 50 cycles, ii) a good capacity retention even at high current rate (~2 A/g) and iii) both extremely low polarization and irreversibility in first cycle for a high loaded electrode (98/1/1 as Pb/PVdF/conductive additive % ratio) [38]. The associated reaction mechanism of Pb with Na-ion can be defined as consecutive reversible phase transitions as follows:

$$Pb \leftrightarrow NaPb_3 \leftrightarrow NaPb \leftrightarrow Na_9Pb_4 \leftrightarrow Na_{15}Pb_4 \qquad (2)$$

The detailed electrochemical performance of Pb anode in Na-ion half-cells is presented in **Fig. S3**. The mechanism of Pb anode in Na ion half/cell was primarily studied by Jow et al. [77], followed by Chevrier et al. [78], altogether supporting the above mentioned reaction mechanism.

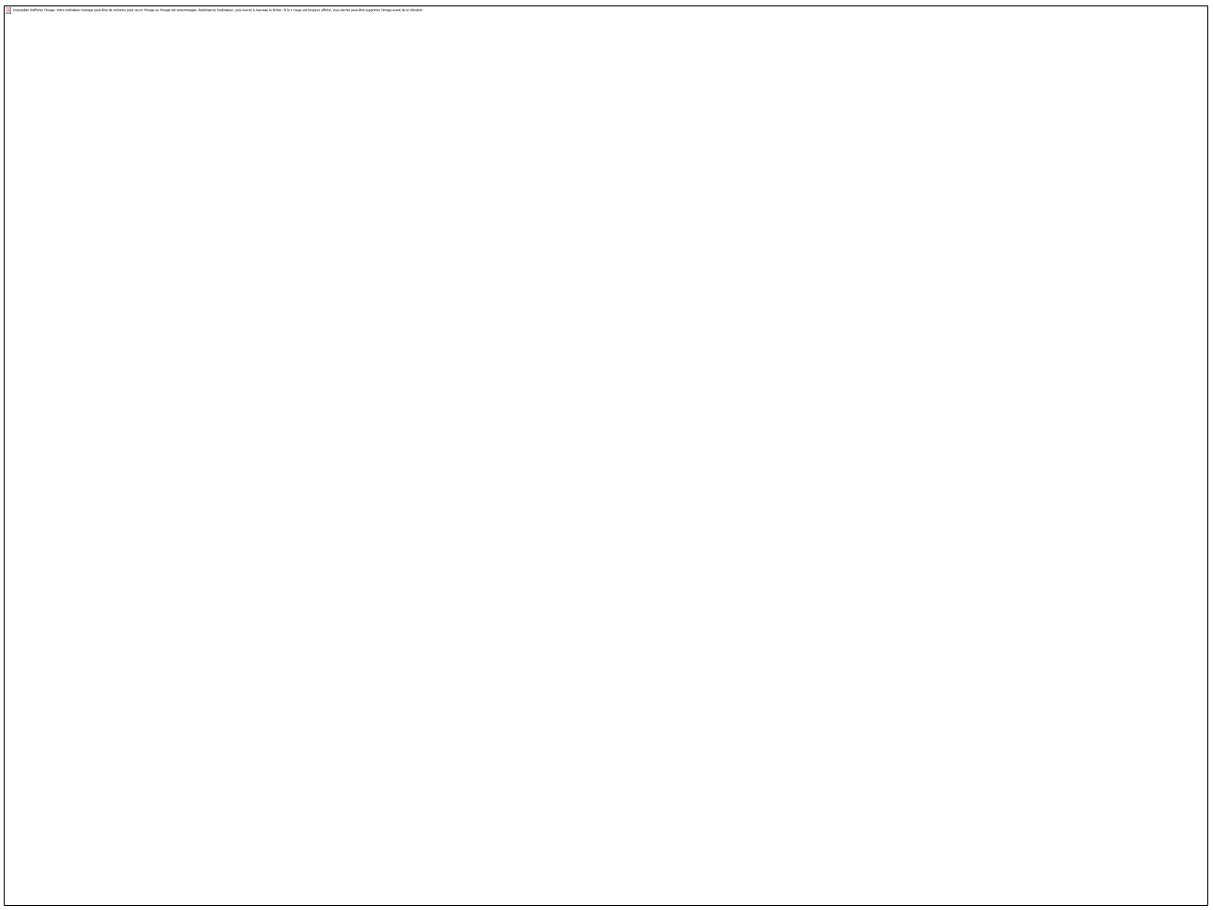

Figure 7 (a) Galvanostatic profiles of NVP-C cathode (black) and Pb anode (red) half-cells versus Na/Na^+. (b) Capacity retention of Pb//NVP-C full coin cell with coulombic efficiency at C/l0. (c) corresponding charge-discharge profiles. (d) magnified view of 75^{th} cycle.

Based on the evaluation of half-cell performance of the NVP-C and Pb electrodes, we assembled full coin-type cell and evaluated their performance. The individual galvanostatic profiles obtained in the full cell, displayed in **Fig. 7a,** are as expected similar to those of the half cells. As NVP-C is the source of Na, to build the full cell the NVP-C cathode mass was overbalanced to compensate the sodium losses in the SEI formation. The full coin cell with NVP-C cathode and Pb anode has a mass loading ratio of 8:1 (vs ~ 4.8:1 for theoretical balance, taking into account the initial irreversible capacities in half-cells). We well recognize in the full cell galvanostatic curve the shape of the NVP plateau (**Fig. 7c and d**) with the

overlap of the four sodiation plateaus coming from Pb anode. From the operando XRD (**Fig. 6**) and the previous study of Pb/Na [38], the following reactions can be proposed:

Pb//NVP-C full cell charge-discharge process:

$$\begin{aligned} &\text{Cathode: } Na_3V_2(PO_4)_3 \underset{\text{Discharge } (+2Na)}{\overset{\text{Charge } (-2Na)}{\leftrightarrow}} NaV_2(PO_4)_3 \\ &\text{Anode: } Pb \underset{\text{Charge } (-3.75Na)}{\overset{\text{Disharge } (+3.75Na)}{\leftrightarrow}} {}^{1}/_{4}\, Na_{15}Pb_4 \end{aligned} \qquad (3)$$

As NVP-C cathode material is used in large excess in full cell, the electrochemical performance of full cell is limited by the Pb anode. Then, capacity values shown here are relative to anode active material (Data considering the active material are given in **Figure S3**). The cell showed a good reversible capacity of 233 mAh/g (**Fig. 7c**). The coulombic efficiency progressively increases and become stable around 99% after 20 cycles (**Fig. 7b**). The CD curves show stable stage-like plateaus, even after 75th cycles, showing good reversibility of the successive sodiation/desodiation process as depicted in **Fig. 7b, c**.

The rate performance of this pioneer full cell using different C-rates starting from C/10 to 10C was tested and are presented in **Fig. S4a**. At the current rates, the reversible capacity of the full cell drops regularly and still recovers (41 %) of initial capacity with an excellent coulombic efficiency of almost 100%. The shape of the CD plots of assembled full cell at different current rates is unchanged up to 2C rate. The full cell delivered a discharge energy density of 170 Wh/kg (by using the mass loading of both NVP-C and Pb electrodes) with sustaining power density of 8 W/kg as specified by Ragone plot in **Fig. S4b**. This value decreases to 18 Wh/kg, with the increase in power density 1165 W/kg. This is comparable with previously reported NVP-C based full cells such as $Na_3V_2(PO_4)_3$//$Na_3V_2(PO_4)_3$ (50–60 Wh/kg) [79], $Na_3V_2(PO_4)_3$//graphite (160–180 Wh/kg) [80], $Na_3V_2(PO_4)_3$//hard carbon (130–

150 Wh/kg) [81], $Na_3V_2(PO_4)_3$//$NaTi_2(PO_4)_3$ (60–80 Wh/kg) [82], Hard carbon//NVPSi-0.05 (342 Wh/kg) [83] and CuS//NVPF/NVP (162.2 Wh/kg) [84]. Moreover, The full cell also shows comparable energy density with other reported Na-ion based full cell systems such as $NaMnO_2$//$NaTi_2(PO_4)_3$/C (30 Wh/kg) [85], NTO nanotube//$VOPO_4$ (220 Wh/kg) [86], Sb@TiO_{2-x}//NVP (151 Wh/kg) [87], Hard carbon//NVPF@rGO (162 Wh/kg) [88], Graphite//$Na_{1.5}VO_{4.8}F_{0.7}$ (149 Wh/kg) [89], and VO_2 nanosheet//NVOPF nanocuboid array (215 Wh/kg) [90] with maintaining good power density at the same time.

In terms of practical aspect, the studied Pb//NVP-C full cell shows moderate performance, and more work should be done to improve both the capacity and its retention. This system Pb/NVPC will represent a promising Na storage system in terms of energy density (gravimetric as well as volumetric) when one will be able to tackle the capacity fading through optimization of both the electrodes balancing and electrolyte formulation.

Conclusions

In summary, a full cell prototype associated with NVP-C and Pb electrodes was designed and evaluated. NVP-C was synthesized through a simple solid-state process, providing a high-performance cathode material for SIB with excellent capacity and stability as well. It was demonstrated that the as-formed cathode exhibited capacity of 104 mAh/g at a current rate of C/10 and an exceptional capacity retention with almost 99.9 % of the first cycle capacity after 3500 cycles vs metallic sodium. Moreover, taking the different reaction kinetics of the Pb anode into consideration, the full Pb//NVP-C SIB showed a reasonable cycle stability for a preliminary study. The assembled full cell demonstrated a reversible capacity of 233 mAh/g at C/10, with an excellent energy density of 170 Wh/kg. This prototype full cells show that the concept gives a real potentiality. No doubt that the moderate

present performance needs to be improved by working on the electrode and electrolyte formulations for instance to counter the soluble degradation products composed at the anode able to diffuse to the cathode (phenomenon pronounced in SIB because of the strong reactivity and solubility of the products) [91], as well as the balancing in the full cell design. In this way we can bridge the gap between lab-made full cell for real-world industry scalable practice full cell. These pioneer results using Pb as negative electrodes in SIB provide an elegant attempt to recycle this element and there is a big room to improve this new and promising concept in near future.

Acknowledgements

The authors are grateful to "Région d'Occitanie" for the financial support through the PLOBANA project (2018-003451).

References

[1] M. Armand, J.M. Tarascon, Building better batteries, Nat., 451 (2008) 652-657.
[2] P.G. Bruce, S.A. Freunberger, L.J. Hardwick, J.-M. Tarascon, Li–O2 and Li–S batteries with high energy storage, Nat. Mater., 11 (2012) 19-29.
[3] J.M. Tarascon, M. Armand, Issues and challenges facing rechargeable lithium batteries, Nat., 414 (2001) 359-367.
[4] S.P. Ong, V.L. Chevrier, G. Hautier, A. Jain, C. Moore, S. Kim, X. Ma, G. Ceder, Voltage, stability and diffusion barrier differences between sodium-ion and lithium-ion intercalation materials, Energy Environ. Sci., 4 (2011) 3680-3688.
[5] S.-W. Kim, D.-H. Seo, X. Ma, G. Ceder, K. Kang, Electrode Materials for Rechargeable Sodium-Ion Batteries: Potential Alternatives to Current Lithium-Ion Batteries, Adv. Energy Mater., 2 (2012) 710-721.
[6] Y. Wang, X. Yu, S. Xu, J. Bai, R. Xiao, Y.-S. Hu, H. Li, X.-Q. Yang, L. Chen, X. Huang, A zero-strain layered metal oxide as the negative electrode for long-life sodium-ion batteries, Nat. Commun., 4 (2013) 2365.
[7] D. Kim, S.-H. Kang, M. Slater, S. Rood, J.T. Vaughey, N. Karan, M. Balasubramanian, C.S. Johnson, Enabling Sodium Batteries Using Lithium-Substituted Sodium Layered Transition Metal Oxide Cathodes, Adv. Energy Mater., 1 (2011) 333-336.
[8] N. Yabuuchi, M. Kajiyama, J. Iwatate, H. Nishikawa, S. Hitomi, R. Okuyama, R. Usui, Y. Yamada, S. Komaba, P2-type Nax[Fe1/2Mn1/2]O2 made from earth-abundant elements for rechargeable Na batteries, Nat. Mater., 11 (2012) 512-517.
[9] J. Billaud, R.J. Clément, A.R. Armstrong, J. Canales-Vázquez, P. Rozier, C.P. Grey, P.G. Bruce, β-NaMnO2: A High-Performance Cathode for Sodium-Ion Batteries, J. Am. Chem. Soc., 136 (2014) 17243-17248.
[10] Y. Cao, L. Xiao, W. Wang, D. Choi, Z. Nie, J. Yu, L.V. Saraf, Z. Yang, J. Liu, Reversible Sodium Ion Insertion in Single Crystalline Manganese Oxide Nanowires with Long Cycle Life, Adv. Mater., 23 (2011) 3155-3160.
[11] D. Yuan, X. Liang, L. Wu, Y. Cao, X. Ai, J. Feng, H. Yang, A Honeycomb-Layered Na3Ni2SbO6: A High-Rate and Cycle-Stable Cathode for Sodium-Ion Batteries, Adv. Mater., 26 (2014) 6301-6306.
[12] S.-M. Oh, S.-T. Myung, J. Hassoun, B. Scrosati, Y.-K. Sun, Reversible NaFePO4 electrode for sodium secondary batteries, Electrochem. Commun., 22 (2012) 149-152.
[13] Y. Fang, L. Xiao, J. Qian, X. Ai, H. Yang, Y. Cao, Mesoporous Amorphous FePO4 Nanospheres as High-Performance Cathode Material for Sodium-Ion Batteries, Nano Lett., 14 (2014) 3539-3543.
[14] Y. Fang, J. Zhang, L. Xiao, X. Ai, Y. Cao, H. Yang, Phosphate Framework Electrode Materials for Sodium Ion Batteries, Adv. Sci., 4 (2017) 1600392.
[15] J. Qian, M. Zhou, Y. Cao, X. Ai, H. Yang, Nanosized Na4Fe(CN)6/C Composite as a Low-Cost and High-Rate Cathode Material for Sodium-Ion Batteries, Adv. Energy Mater., 2 (2012) 410-414.
[16] L. Wang, Y. Lu, J. Liu, M. Xu, J. Cheng, D. Zhang, J.B. Goodenough, A Superior Low-Cost Cathode for a Na-Ion Battery, Angew. Chem. Int. Ed., 52 (2013) 1964-1967.
[17] H. Zhou, M.-A. Einarsrud, F. Vullum-Bruer, High capacity nanostructured Li2FexSiO4/C with Fe hyperstoichiometry for Li-ion batteries, J. Power Sources, 235 (2013) 234-242.
[18] L. Zhang, T. Huang, A. Yu, Carbon-coated Na3V2(PO4)3 nanocomposite as a novel high rate cathode material for aqueous sodium ion batteries, J. Alloys Compd., 646 (2015) 522-527.
[19] J. Fang, S. Wang, Z. Li, H. Chen, L. Xia, L. Ding, H. Wang, Porous Na3V2(PO4)3@C nanoparticles enwrapped in three-dimensional graphene for high performance sodium-ion batteries, J. Mater. Chem. A, 4 (2016) 1180-1185.
[20] M.J. Aragón, P. Lavela, G.F. Ortiz, J.L. Tirado, Effect of Iron Substitution in the Electrochemical Performance of Na3V2(PO4)3as Cathode for Na-Ion Batteries, J. Electrochem. Soc., 162 (2015) A3077-A3083.

[21] R. Klee, P. Lavela, M.J. Aragón, R. Alcántara, J.L. Tirado, Enhanced high-rate performance of manganese substituted Na3V2(PO4)3/C as cathode for sodium-ion batteries, J. Power Sources, 313 (2016) 73-80.
[22] H. Li, X. Yu, Y. Bai, F. Wu, C. Wu, L.-Y. Liu, X.-Q. Yang, Effects of Mg doping on the remarkably enhanced electrochemical performance of Na3V2(PO4)3 cathode materials for sodium ion batteries, J. Mater. Chem. A, 3 (2015) 9578-9586.
[23] H. Li, Y. Bai, F. Wu, Y. Li, C. Wu, Budding willow branches shaped Na3V2(PO4)3/C nanofibers synthesized via an electrospinning technique and used as cathode material for sodium ion batteries, J. Power Sources, 273 (2015) 784-792.
[24] S. Kajiyama, J. Kikkawa, J. Hoshino, M. Okubo, E. Hosono, Assembly of Na3V2(PO4)3 Nanoparticles Confined in a One-Dimensional Carbon Sheath for Enhanced Sodium-Ion Cathode Properties, Chem. Eur. J., 20 (2014) 12636-12640.
[25] Y. Jiang, Z. Yang, W. Li, L. Zeng, F. Pan, M. Wang, X. Wei, G. Hu, L. Gu, Y. Yu, Nanoconfined Carbon-Coated Na3V2(PO4)3 Particles in Mesoporous Carbon Enabling Ultralong Cycle Life for Sodium-Ion Batteries, Adv. Energy Mater., 5 (2015) 1402104.
[26] C. Zhu, K. Song, P.A. van Aken, J. Maier, Y. Yu, Carbon-Coated Na3V2(PO4)3 Embedded in Porous Carbon Matrix: An Ultrafast Na-Storage Cathode with the Potential of Outperforming Li Cathodes, Nano Lett., 14 (2014) 2175-2180.
[27] X. Rui, W. Sun, C. Wu, Y. Yu, Q. Yan, An Advanced Sodium-Ion Battery Composed of Carbon Coated Na3V2(PO4)3 in a Porous Graphene Network, Adv. Mater., 27 (2015) 6670-6676.
[28] S. Tao, P. Cui, W. Huang, Z. Yu, X. Wang, S. Wei, D. Liu, L. Song, W. Chu, Sol–gel design strategy for embedded Na3V2(PO4)3 particles into carbon matrices for high-performance sodium-ion batteries, Carbon, 96 (2016) 1028-1033.
[29] Z. Jian, L. Zhao, H. Pan, Y.-S. Hu, H. Li, W. Chen, L. Chen, Carbon coated Na3V2(PO4)3 as novel electrode material for sodium ion batteries, Electrochem. Commun., 14 (2012) 86-89.
[30] S.Y. Lim, H. Kim, R.A. Shakoor, Y. Jung, J.W. Choi, Electrochemical and Thermal Properties of NASICON Structured Na3V2(PO4)3as a Sodium Rechargeable Battery Cathode: A Combined Experimental and Theoretical Study, J. Electrochem. Soc., 159 (2012) A1393-A1397.
[31] Y.H. Jung, C.H. Lim, D.K. Kim, Graphene-supported Na3V2(PO4)3 as a high rate cathode material for sodium-ion batteries, J. Mater. Chem. A, 1 (2013) 11350-11354.
[32] M. Martos, J. Morales, L. Sánchez, Lead-based systems as suitable anode materials for Li-ion batteries, Electrochim. Acta, 48 (2003) 615-621.
[33] L.D. Ellis, B.N. Wilkes, T.D. Hatchard, M.N. Obrovac, In Situ XRD Study of Silicon, Lead and Bismuth Negative Electrodes in Nonaqueous Sodium Cells, J. Electrochem. Soc., 161 (2014) A416-A421.
[34] V. Gabaudan, R. Berthelot, L. Stievano, L. Monconduit, Electrochemical Alloying of Lead in Potassium-Ion Batteries, ACS Omega, 3 (2018) 12195-12200.
[35] X. Lin, P. Li, L. Shao, X. Zheng, M. Shui, N. Long, D. Wang, J. Shu, CNT-enhanced electrochemical property and sodium storage mechanism of Pb(NO3)2 as anode material for Na-ion batteries, Electrochim. Acta, 169 (2015) 382-394.
[36] R.A. Huggins, Alternative materials for negative electrodes in lithium systems, Solid State Ionics, 152-153 (2002) 61-68.
[37] W.-J. Zhang, A review of the electrochemical performance of alloy anodes for lithium-ion batteries, J. Power Sources, 196 (2011) 13-24.
[38] A. Darwiche, R. Dugas, B. Fraisse, L. Monconduit, Reinstating lead for high-loaded efficient negative electrode for rechargeable sodium-ion battery, J. Power Sources, 304 (2016) 1-8.
[39] B. Pandit, S.R. Rondiya, N.Y. Dzade, S.F. Shaikh, N. Kumar, E.S. Goda, A.A. Al-Kahtani, R.S. Mane, S. Mathur, R.R. Salunkhe, High Stability and Long Cycle Life of Rechargeable Sodium-Ion Battery Using Manganese Oxide Cathode: A Combined Density Functional Theory (DFT) and Experimental Study, ACS Appl. Mater. Interfaces, 13 (2021) 11433-11441.

[40] J.B. Leriche, S. Hamelet, J. Shu, M. Morcrette, C. Masquelier, G. Ouvrard, M. Zerrouki, P. Soudan, S. Belin, E. Elkaïm, F. Baudelet, An Electrochemical Cell for Operando Study of Lithium Batteries Using Synchrotron Radiation, J. Electrochem. Soc., 157 (2010) A606.
[41] J. Rodríguez-Carvajal, Recent advances in magnetic structure determination by neutron powder diffraction, Physica B: Condensed Matter, 192 (1993) 55-69.
[42] S. Li, P. Ge, C. Zhang, W. Sun, H. Hou, X. Ji, The electrochemical exploration of double carbon-wrapped Na3V2(PO4)3: Towards long-time cycling and superior rate sodium-ion battery cathode, J. Power Sources, 366 (2017) 249-258.
[43] C. Delmas, R. Olazcuaga, F. Cherkaoui, R. Brochu, G. Le Flem, A new family of phosphates with the formula Na3M2 (PO4) 3 (M= TI, V, Cr, Fe), Chemischer Informationsdienst, 10 (1979) no-no.
[44] E. Gu, S. Liu, Z. Zhang, Y. Fang, X. Zhou, J. Bao, An efficient sodium-ion battery consisting of reduced graphene oxide bonded Na3V2(PO4)3 in a composite carbon network, J. Alloys Compd., 767 (2018) 131-140.
[45] Y. Zhang, A. Pan, Y. Wang, X. Cao, Z. Zhou, T. Zhu, S. Liang, G. Cao, Self-templated synthesis of N-doped CoSe2/C double-shelled dodecahedra for high-performance supercapacitors, Energy Storage Mater., 8 (2017) 28-34.
[46] Z. Jian, W. Han, X. Lu, H. Yang, Y.-S. Hu, J. Zhou, Z. Zhou, J. Li, W. Chen, D. Chen, L. Chen, Superior Electrochemical Performance and Storage Mechanism of Na3V2(PO4)3 Cathode for Room-Temperature Sodium-Ion Batteries, Adv. Energy Mater., 3 (2013) 156-160.
[47] J. Xu, E. Gu, Z. Zhang, Z. Xu, Y. Xu, Y. Du, X. Zhu, X. Zhou, Fabrication of porous Na3V2(PO4)3/reduced graphene oxide hollow spheres with enhanced sodium storage performance, J. Colloid Interface Sci., 567 (2020) 84-91.
[48] W. He, X. Zhang, X. Du, Y. Zhang, Y. Yue, J. Shen, M. Li, Bio-assisted synthesis of mesoporous Li3V2(PO4)3 for high performance lithium-ion batteries, Electrochim. Acta, 112 (2013) 295-303.
[49] B. Liu, S. Ke, Y. Shao, D. Jia, C. Fan, F. Zhang, R. Fan, Formation mechanism for oxidation synthesis of carbon nanomaterials and detonation process for core-shell structure, Carbon, 127 (2018) 21-30.
[50] X. Cao, A. Pan, B. Yin, G. Fang, Y. Wang, X. Kong, T. Zhu, J. Zhou, G. Cao, S. Liang, Nanoflake-constructed porous Na3V2(PO4)3/C hierarchical microspheres as a bicontinuous cathode for sodium-ion batteries applications, Nano Energy, 60 (2019) 312-323.
[51] M. Yu, Y. Zeng, Y. Han, X. Cheng, W. Zhao, C. Liang, Y. Tong, H. Tang, X. Lu, Valence-Optimized Vanadium Oxide Supercapacitor Electrodes Exhibit Ultrahigh Capacitance and Super-Long Cyclic Durability of 100 000 Cycles, Adv. Funct. Mater., 25 (2015) 3534-3540.
[52] M.V. Reddy, G.V. Subba Rao, B.V.R. Chowdari, Long-term cycling studies on 4V-cathode, lithium vanadium fluorophosphate, J. Power Sources, 195 (2010) 5768-5774.
[53] Z. Wang, J. Liu, Z. Du, H. Tao, Y. Yue, Enhancing Na-ion storage in Na3V2(PO4)3/C cathodes for sodium ion batteries through Br and N co-doping, Inorg. Chem. Front., 7 (2020) 1289-1297.
[54] Y.Z. Dong, Y.M. Zhao, H. Duan, The effect of doping Mg2+ on the structure and electrochemical properties of Li3V2(PO4)3 cathode materials for lithium-ion batteries, J. Electroanal. Chem., 660 (2011) 14-21.
[55] R. Rajagopalan, L. Zhang, S.X. Dou, H.K. Liu, Tuned In Situ Growth of Nanolayered rGO on 3D Na3V2(PO4)3 Matrices: A Step toward Long Lasting, High Power Na-Ion Batteries, Adv. Mater. Interfaces, 3 (2016) 1600007.
[56] E. Boivin, J.-N. Chotard, C. Masquelier, L. Croguennec, Towards Reversible High-Voltage Multi-Electron Reactions in Alkali-Ion Batteries Using Vanadium Phosphate Positive Electrode Materials, Molecules, 26 (2021) 1428.
[57] C. Zhang, J. Wan, Y. Li, S. Zheng, K. Zhou, D. Wang, D. Wang, C. Hong, Z. Gong, Y. Yang, Restraining the polarization increase of Ni-rich and low-Co cathodes upon cycling by Al-doping, J. Mater. Chem. A, 8 (2020) 6893-6901.
[58] T.-F. Hung, W.-J. Cheng, W.-S. Chang, C.-C. Yang, C.-C. Shen, Y.-L. Kuo, Ascorbic Acid-Assisted Synthesis of Mesoporous Sodium Vanadium Phosphate Nanoparticles with Highly sp2-Coordinated

Carbon Coatings as Efficient Cathode Materials for Rechargeable Sodium-Ion Batteries, Chem. Eur. J., 22 (2016) 10620-10626.
[59] S. Li, Y. Dong, L. Xu, X. Xu, L. He, L. Mai, Effect of Carbon Matrix Dimensions on the Electrochemical Properties of Na3V2(PO4)3 Nanograins for High-Performance Symmetric Sodium-Ion Batteries, Adv. Mater., 26 (2014) 3545-3553.
[60] C.V. Manohar, A. Raj K, M. Kar, M. Forsyth, D.R. MacFarlane, S. Mitra, Stability enhancing ionic liquid hybrid electrolyte for NVP@C cathode based sodium batteries, Sustain. Energy Fuels, 2 (2018) 566-576.
[61] J. Xu, J. Chen, S. Zhou, C. Han, M. Xu, N. Zhao, C.-P. Wong, Sequentially-processed Na3V2(PO4)3 for cathode material of aprotic sodium ion battery, Nano Energy, 50 (2018) 323-330.
[62] S.-h. Luo, J.-y. Li, S. Bao, Y.-y. Liu, Z. Wang, Na3V2(PO4)3/C Composite Prepared by Sol-Gel Method as Cathode for Sodium Ion Batteries, J. Electrochem. Soc., 165 (2018) A1460-A1465.
[63] G. Li, D. Jiang, H. Wang, X. Lan, H. Zhong, Y. Jiang, Glucose-assisted synthesis of Na3V2(PO4)3/C composite as an electrode material for high-performance sodium-ion batteries, J. Power Sources, 265 (2014) 325-334.
[64] X. Yao, Z. Zhu, Q. Li, X. Wang, X. Xu, J. Meng, W. Ren, X. Zhang, Y. Huang, L. Mai, 3.0 V High Energy Density Symmetric Sodium-Ion Battery: Na4V2(PO4)3‖Na3V2(PO4)3, ACS Appl. Mater. Interfaces, 10 (2018) 10022-10028.
[65] A. Chekannikov, R. Kapaev, S. Novikova, N. Tabachkova, T. Kulova, A. Skundin, A. Yaroslavtsev, Na3V2(PO4)3/C/Ag nanocomposite materials for Na-ion batteries obtained by the modified Pechini method, J. Solid State Electrochem., 21 (2017) 1615-1624.
[66] J. Zhang, T. Yuan, H. Wan, J. Qian, X. Ai, H. Yang, Y. Cao, Surface-engineering enhanced sodium storage performance of Na3V2(PO4)3 cathode via in-situ self-decorated conducting polymer route, Sci. China Chem., 60 (2017) 1546-1553.
[67] J. Yang, D.-W. Han, M.R. Jo, K. Song, Y.-I. Kim, S.-L. Chou, H.-K. Liu, Y.-M. Kang, Na3V2(PO4)3 particles partly embedded in carbon nanofibers with superb kinetics for ultra-high power sodium ion batteries, J. Mater. Chem. A, 3 (2015) 1005-1009.
[68] R. Klee, M.J. Aragón, P. Lavela, R. Alcántara, J.L. Tirado, Na3V2(PO4)3/C Nanorods with Improved Electrode–Electrolyte Interface As Cathode Material for Sodium-Ion Batteries, ACS Appl. Mater. Interfaces, 8 (2016) 23151-23159.
[69] Z. Jian, C. Yuan, W. Han, X. Lu, L. Gu, X. Xi, Y.-S. Hu, H. Li, W. Chen, D. Chen, Y. Ikuhara, L. Chen, Atomic Structure and Kinetics of NASICON NaxV2(PO4)3 Cathode for Sodium-Ion Batteries, Adv. Funct. Mater., 24 (2014) 4265-4272.
[70] X. Liang, X. Ou, F. Zheng, Q. Pan, X. Xiong, R. Hu, C. Yang, M. Liu, Surface Modification of Na3V2(PO4)3 by Nitrogen and Sulfur Dual-Doped Carbon Layer with Advanced Sodium Storage Property, ACS Appl. Mater. Interfaces, 9 (2017) 13151-13162.
[71] S. Islam, M.H. Alfaruqi, D.Y. Putro, V. Mathew, S. Kim, J. Jo, S. Kim, Y.-K. Sun, K. Kim, J. Kim, Pyrosynthesis of Na3V2(PO4)3@C Cathodes for Safe and Low-Cost Aqueous Hybrid Batteries, ChemSusChem, 11 (2018) 2239-2247.
[72] P. Hu, Z. Zou, X. Sun, D. Wang, J. Ma, Q. Kong, D. Xiao, L. Gu, X. Zhou, J. Zhao, S. Dong, B. He, M. Avdeev, S. Shi, G. Cui, L. Chen, Uncovering the Potential of M1-Site-Activated NASICON Cathodes for Zn-Ion Batteries, Adv. Mater., 32 (2020) 1907526.
[73] S.K. Pal, R. Thirupathi, S. Chakrabarty, S. Omar, Improving the Electrochemical Performance of Na3V2(PO4)3 Cathode in Na-Ion Batteries by Si-Doping, ACS Appl. Energy Mater., 3 (2020) 12054-12065.
[74] M.J. Aragón, P. Lavela, G.F. Ortiz, J.L. Tirado, Benefits of Chromium Substitution in Na3V2(PO4)3 as a Potential Candidate for Sodium-Ion Batteries, ChemElectroChem, 2 (2015) 995-1002.
[75] F. Lalère, V. Seznec, M. Courty, R. David, J.N. Chotard, C. Masquelier, Improving the energy density of Na3V2(PO4)3-based positive electrodes through V/Al substitution, J. Mater. Chem. A, 3 (2015) 16198-16205.

[76] C.W. Mason, I. Gocheva, H.E. Hoster, D.Y.W. Yu, Activating Vanadium's Highest Oxidation State in the NASICON Structure, ECS Trans., 58 (2014) 41-46.
[77] T.R. Jow, L.W. Shacklette, M. Maxfield, D. Vernick, The Role of Conductive Polymers in Alkali-Metal Secondary Electrodes, J. Electrochem. Soc., 134 (1987) 1730-1733.
[78] V.L. Chevrier, G. Ceder, Challenges for Na-ion Negative Electrodes, J. Electrochem. Soc., 158 (2011) A1011.
[79] Y. Zhang, H. Zhao, Y. Du, Symmetric full cells assembled by using self-supporting Na3V2(PO4)3 bipolar electrodes for superior sodium energy storage, J. Mater. Chem. A, 4 (2016) 7155-7159.
[80] P. Han, X. Han, J. Yao, Z. Liu, X. Cao, G. Cui, Flexible graphite film with laser drilling pores as novel integrated anode free of metal current collector for sodium ion battery, Electrochem. Commun., 61 (2015) 84-88.
[81] Z. Yuan, L. Si, X. Zhu, Three-dimensional hard carbon matrix for sodium-ion battery anode with superior-rate performance and ultralong cycle life, J. Mater. Chem. A, 3 (2015) 23403-23411.
[82] W. Ren, Z. Zheng, C. Xu, C. Niu, Q. Wei, Q. An, K. Zhao, M. Yan, M. Qin, L. Mai, Self-sacrificed synthesis of three-dimensional Na3V2(PO4)3 nanofiber network for high-rate sodium–ion full batteries, Nano Energy, 25 (2016) 145-153.
[83] M.J. Aragón, P. Lavela, G.F. Ortiz, R. Alcántara, J.L. Tirado, On the Effect of Silicon Substitution in Na3V2(PO4)3 on the Electrochemical Behavior as Cathode for Sodium-Ion Batteries, ChemElectroChem, 5 (2018) 367-374.
[84] J.Y. Park, Y. Shim, Y.-i. Kim, Y. Choi, H.J. Lee, J. Park, J.E. Wang, Y. Lee, J.H. Chang, K. Yim, C.W. Ahn, C.-W. Lee, D.K. Kim, J.M. Yuk, An iron-doped NASICON type sodium ion battery cathode for enhanced sodium storage performance and its full cell applications, J. Mater. Chem. A, 8 (2020) 20436-20445.
[85] Z. Hou, X. Li, J. Liang, Y. Zhu, Y. Qian, An aqueous rechargeable sodium ion battery based on a NaMnO2–NaTi2(PO4)3 hybrid system for stationary energy storage, J. Mater. Chem. A, 3 (2015) 1400-1404.
[86] H. Li, L. Peng, Y. Zhu, D. Chen, X. Zhang, G. Yu, An advanced high-energy sodium ion full battery based on nanostructured Na2Ti3O7/VOPO4 layered materials, Energy Environ. Sci., 9 (2016) 3399-3405.
[87] N. Wang, Z. Bai, Y. Qian, J. Yang, Double-Walled Sb@TiO2−x Nanotubes as a Superior High-Rate and Ultralong-Lifespan Anode Material for Na-Ion and Li-Ion Batteries, Adv. Mater., 28 (2016) 4126-4133.
[88] F. Li, Y. Zhao, L. Xia, Z. Yang, J. Wei, Z. Zhou, Well-dispersed Na3V2(PO4)2F3@rGO with improved kinetics for high-power sodium-ion batteries, J. Mater. Chem. A, 8 (2020) 12391-12397.
[89] Z.-L. Xu, G. Yoon, K.-Y. Park, H. Park, O. Tamwattana, S. Joo Kim, W.M. Seong, K. Kang, Tailoring sodium intercalation in graphite for high energy and power sodium ion batteries, Nat. Commun., 10 (2019) 2598.
[90] D. Chao, C.-H. Lai, P. Liang, Q. Wei, Y.-S. Wang, C. Zhu, G. Deng, V.V.T. Doan-Nguyen, J. Lin, L. Mai, H.J. Fan, B. Dunn, Z.X. Shen, Sodium Vanadium Fluorophosphates (NVOPF) Array Cathode Designed for High-Rate Full Sodium Ion Storage Device, Adv. Energy Mater., 8 (2018) 1800058.
[91] O.C. Harris, S.E. Lee, C. Lees, M. Tang, Review: mechanisms and consequences of chemical cross-talk in advanced Li-ion batteries, J. Phys. Energy, 2 (2020) 032002.